

Episodic Southern Ocean heat loss and its mixed layer impacts revealed by the furthest south multi-year surface flux mooring

S. E. Ogle¹, V. Tamsitt¹, S. A. Josey², S. T. Gille¹, I. Cerovečki¹, L. D. Talley¹ and R. A. Weller³

¹Scripps Institution of Oceanography, La Jolla, California 92093, USA

²National Oceanography Centre, Southampton, UK

³Woods Hole Oceanographic Institution, Woods Hole, MA, USA

Key Points:

- The southernmost long-term open ocean mooring yields the first multi-year air-sea flux results south of 50°S.
- Episodic turbulent heat loss events occur year-round, and are driven primarily by cold, dry northeastward winds.
- Winter 2015 had more intense heat loss events, deeper mixed layers, and greater Subantarctic Mode Water formation than 2016.

Abstract

The Ocean Observatories Initiative (OOI) air-sea flux mooring deployed at 54.08°S, 89.67°W, in the southeast Pacific sector of the Southern Ocean, is the furthest south long-term open ocean flux mooring ever deployed. Mooring observations (Feb 2015-Aug 2017) provide the first in-situ quantification of annual net air-sea heat exchange from one of the prime Subantarctic Mode Water (SAMW) formation regions. Episodic turbulent heat loss events (reaching a daily mean net flux of -294 W m^{-2}) generally occur when northeastward winds bring relatively cold, dry air to the mooring location, leading to large air-sea temperature and humidity differences. Wintertime heat loss events promote deep mixed layer formation that lead to SAMW formation. However, these processes have strong interannual variability; a higher frequency of $2\text{-}\sigma$ and $3\text{-}\sigma$ turbulent heat loss events in winter 2015 led to deep mixed layers ($>300 \text{ m}$), which were nonexistent in winter 2016.

1 Introduction

The Southern Ocean is a vital part of the Earth system that connects the world's oceans and is a key site for water mass formation [Judicone *et al.*, 2008; Talley *et al.*, 2011]; it accounts for 40-50% of global oceanic uptake of anthropogenic CO_2 [Sabine *et al.*, 2004; Mikaloff Fletcher *et al.*, 2006; Frölicher *et al.*, 2015] and 75% of anthropogenic heat [Dufour *et al.*, 2015; Frölicher *et al.*, 2015]. Much of this uptake occurs north of the Antarctic Circumpolar Current (ACC) where wintertime net surface ocean heat loss and vigorous mixing result in formation of deep mixed layers [McCartney, 1977, 1982; Naveira Garabato *et al.*, 2009; Holte *et al.*, 2012]. These deep winter mixed layers subduct into the ocean interior forming relatively oxygen-rich, anthropogenic CO_2 -rich SAMW [Sabine *et al.*, 2004; Ito *et al.*, 2010]. The deepest MLDs ($>500 \text{ m}$) develop north of the Subantarctic Front (SAF), the northernmost front of the ACC, in the Southeast Pacific and Indian Oceans [Hanawa and Talley, 2001; Lenton and Matear, 2007; Hartin *et al.*, 2011; Cerovečki *et al.*, 2013].

Wintertime surface ocean heat loss, driven primarily by turbulent (latent and sensible) heat flux, is the main mechanism causing SAMW formation [Holte *et al.*, 2012; Cerovečki and Mazloff, 2016]. Limited observations in the Southeast Pacific suggest that turbulent heat loss events associated with storms may be an important driver for winter mixed layer deepening [Holte *et al.*, 2012]. Hence, characterizing air-sea heat flux variability in the Southern Ocean is a key step for understanding the formation and variability of SAMW. Unfortunately, ship observations of variables (near surface air temperature and humidity, sea surface temperature and wind speed) required to determine turbulent heat loss are extremely sparse in the Southern Ocean, particularly in winter [Figure 1; see also Figure 1 of Gille *et al.*, 2016]. As a result, the Southern Ocean has been the least observed ocean and therefore is a major source of uncertainty in the global heat budget [da Silva *et al.*, 1994; Josey *et al.*, 2013; Bourassa *et al.*, 2013].

Consequently, until now, it has not been possible to analyze the relationship between SAMW formation and air-sea heat exchange using reliable, year-round observations. The OOI Southern Ocean mooring array, deployed in February 2015, provides the first high-quality time series of the surface fluxes and subsurface ocean properties in a key SAMW formation region [Cerovečki *et al.*, 2013; Holte *et al.*, 2017] (Figure 1a). The array is located north of the SAF, and contains the farthest south, long-term, open ocean air-sea flux mooring ever deployed. Observations offer the first opportunity to quantify the annual cycle of air-sea fluxes from such a high southern latitude, to analyze episodic turbulent heat loss events in relation to deep mixed layer formation, and to contrast the observations from two years with very different climate conditions.

We describe the data and methods in section 2, analyze the mooring heat flux variability in section 3.1, and characterize heat loss events within the context of atmospheric regimes in section 3.2. Discussion and conclusions are given in section 4.

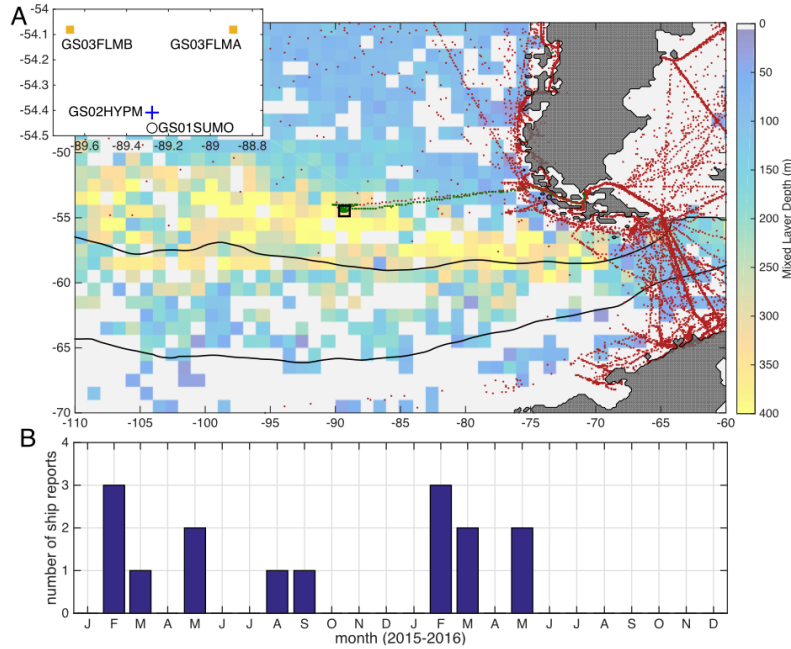


Figure 1. a) Map of region near the OOI mooring array (black rectangle) with the climatological monthly mean August mixed layer depth (MLD) (color) from Argo floats [Holte *et al.*, 2017]. Light gray regions have no August Argo observations. Black lines show the mean position of the Subantarctic and Polar Fronts (PF-M and SAF-M) from Sokolov and Rintoul [2009]. Dark green dots show the locations of flux measurements during the initial OOI mooring deployment cruise in February 2015, and red dots show the location of individual ship-based meteorological reports in the ICOADS3.0 dataset [Freeman *et al.*, 2017] with sufficient data to estimate latent heat flux obtained during all months of 2015 and 2016. The inset map shows the position of the OOI surface mooring (GS01SUMO), profiler mooring (GS02HYPM), and flanking moorings (GS03FLMA and GS03FLMB); b) total number of ship-based meteorological reports in the ICOADS3.0 dataset with sufficient data to estimate latent heat flux obtained within 500 km of the OOI mooring site for each month of 2015 and 2016, excluding all OOI mooring deployment and recovery cruises.

2 Data and Methods

The OOI Apex Surface Mooring (OOI site ID GS01SUMO, hereafter referred to as the surface mooring) is co-located with the Apex Profiler Mooring (GS02HYPM, hereafter referred to as the profiler mooring) at 54.47°S, 89.28°W in the southeast Pacific sector of the Southern Ocean, anchored at 4800 m. Flanking Subsurface Mooring A (GS03FLMA) located at 54.08°S, 88.89°W and Flanking Subsurface Mooring B (GS03FLMB) located at 54.08°S, 89.67°W are each 55 km from the surface mooring, forming a triangular configuration (Figure 1a, inset). There were three approximately year-long mooring deployments: the first deployed in February 2015, the second in December 2015, and the third in November 2016. Although weather prevented the scheduled removal of the surface mooring in December 2017, no maintenance was performed in 2017.

The surface mooring is mounted with duplicate Star Engineering ASIMET packages (OOI data streams METBK11 and METBK12), which return 1-minute average measurements of air temperature, air humidity, barometric pressure, precipitation, northward and eastward wind components, and downwelling shortwave and longwave irradiance. The ASIMET package was developed to obtain climate quality surface meteorological and air-sea flux observations for periods of a year and longer [Hosom *et al.*, 1995]. Analysis of

measurement quality has been done for mid-latitudes by *Colbo and Weller* [2009] and for a Gulf Stream location [*Weller et al.*, 2012; *Bigorre et al.*, 2013]. The OOI surface mooring was further optimized for this location by increasing the mast and placing the meteorological sensors roughly 5 m above the sea surface. Including all measurement errors and uncertainties in the bulk formulae, even during cold air outbreaks in the winter, errors in the derived flux components, net heat flux, and wind stress were 20% or less and closer to 10% in high winds.

The buoy is mounted with a CTD instrument at approximately 1 m below the sea surface to measure sea surface temperature (SST) and sea surface salinity. The surface mooring has a subsurface CTD mounted on a near surface instrument frame at 12 m depth, and 14 CTDs (not used due to insufficient data) to 1500 m depth. The profiler mooring is co-located with the surface mooring, and contains two wire-following McLane Moored Profilers that provide CTD profiles below 180 m. The two flanking subsurface moorings are each mounted with 12 fixed depth CTDs between 30 m and 1500 m. Proper functioning and measurement quality of the mooring sensors were assessed by comparison with shipboard measurements taken near the moorings during deployment and recovery cruises.

The net air-sea heat flux (Q_{NET} , positive into the ocean), net shortwave radiation (Q_{SW}), net longwave radiation (Q_{LW}), sensible heat flux (Q_{SH}), and latent heat flux (Q_{LH}) are calculated from METBK11 and METBK12 using a modified version of the COARE 3.5 flux algorithm from *Edson et al.* [2013] (documented at <https://github.com/ooici>). Precipitation that differs in temperature from SST can induce an additional contribution to net heat flux; however, this term is small at most times (mean over the full time series is 3 W m^{-2} and standard deviation is 3 W m^{-2}), so it is not shown but is included in the net flux calculation. The mooring data processing is described in Supporting Information Text S1 and Table S1 [*Weller et al.*, 2015; *Bigorre et al.*, 2017; *Curry et al.*, 2017].

We compiled Argo float profiles [e.g. *Roemmich et al.*, 2009] near the mooring (within the region 52.5-57.5°S and 85-95°W) from February 1, 2015 through August 15, 2017, yielding 396 profiles. Mixed layer depth (MLD) estimates from the floats and mooring array are described in Supporting Information Text S2 [*de Boyer Montégut et al.*, 2004].

There are significant gaps in the mooring surface flux data coverage, particularly in 2015. The most continuous data runs from Nov 2015 to Oct 2016, with the exception of three of the four components (Q_{LH} , Q_{SH} and Q_{LW}) which are not available in Nov 2015. In order to complete the annual cycle and compute annual means (Sec 3.1), we apply OOI based corrections to the NCEP-NCAR Reanalysis1 estimates of these three components in Nov 2015, described in Supplementary Text S3 [*Kalnay et al.*, 1996]. Additionally, we have used the ERA-Interim Reanalysis [*Simmons et al.*, 2007] heat flux estimates to look at snapshots of turbulent heat flux, air temperature, SST, and mean sea level pressure (SLP) to provide the synoptic regime context for the mooring observations [*Dee et al.*, 2011].

3 Results

3.1 Heat Flux Means and Variability

The mooring observations reveal a rich range of surface variability at sub-monthly timescales, a strong seasonal cycle, and significant interannual variability. Daily and monthly mean values for net heat flux and each heat flux component from February 2015 through August 2017 are shown in Figure 2. On sub-monthly timescales, variability in net heat exchange is primarily driven by episodic turbulent heat loss resulting in daily net heat loss as low as -294 W m^{-2} .

Monthly means show a noticeable seasonal cycle in Q_{NET} with ocean heat gain generally from Oct-Mar (maximum: 152 W m^{-2} in January 2016) and heat loss generally

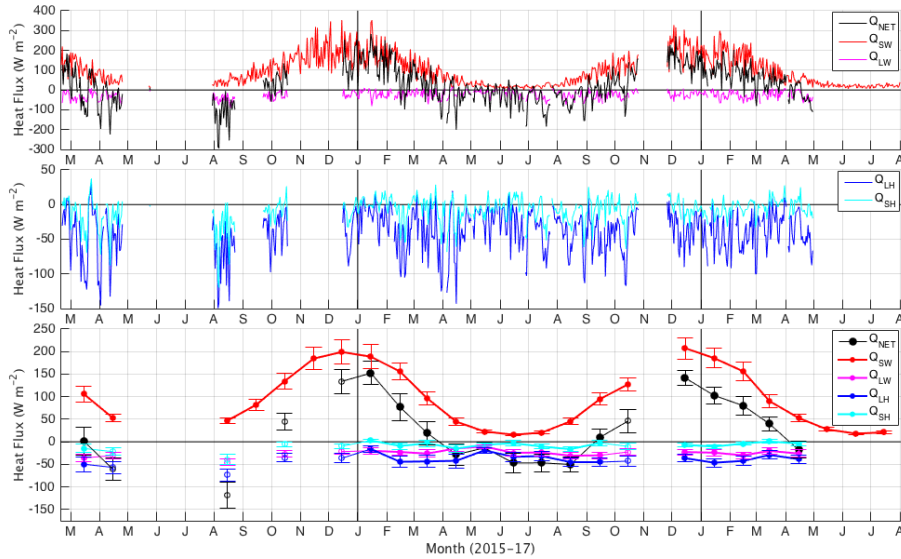


Figure 2. a) Surface mooring average daily heat flux where positive is into the ocean, (Q_{NET} is black, Q_{SW} is red, Q_{LW} is magenta; b) Q_{SH} is cyan, and Q_{LH} is blue); c) mean monthly heat flux calculated in months with five or fewer missing days (solid points) and fifteen or fewer missing days (open circles). Error bars on monthly means represent the standard error of the mean, using a decorrelation time scale of four days to determine the effective number of degrees of freedom.

from Apr-Sep (minimum with limited data: -118 W m^{-2} in August 2015). The limited data for winter 2015 (only August has all flux components available) compared to winter 2016 prevents a full comparison of these two winters. Nevertheless, the available data show that the net heat loss in Aug 2015 was more than twice that of Aug 2016 (-50 W m^{-2}). This indicates strong interannual variability in surface forcing, which can favor or inhibit SAMW formation (see Sec 3.2).

The seasonal cycle in Q_{NET} is evident when continuous observations are available from late 2015 to late 2016. It is primarily caused by strong variation in Q_{SW} (from $<50 \text{ W m}^{-2}$ in winter to approaching 200 W m^{-2} in summer). The Q_{LH} , Q_{SH} , and Q_{LW} terms remain relatively constant year-round in 2016, varying by at most 30 W m^{-2} in the case of the latent heat flux. However, strong losses in late winter 2015 indicate that these terms may experience a significant seasonal cycle in other years.

We use the period Nov 2015 to Oct 2016 to determine annual mean surface flux. The values obtained are $Q_{LH}=-37$, $Q_{SH}=-8$, $Q_{LW}=-23$, and $Q_{SW}=99 \text{ W m}^{-2}$, resulting in an annual net heat flux of 29 W m^{-2} . Thus, the ocean is gaining heat at the surface mooring during this time period. However, much stronger heat loss in winter 2015 than in winter 2016 indicates that annually averaged net heat flux at this location may differ substantially and even change sign from year to year.

3.2 Episodic Heat Loss Events

Turbulent heat loss events are evident in the daily time series throughout much of the year with increasing frequency in winter. The mean turbulent heat flux, averaged over the entire time period, is -48 W m^{-2} , with a standard deviation (σ) of the same magnitude, 48 W m^{-2} . The distribution is left skewed and has a 0.25 quantile of -72 W m^{-2} , a median of -36 W m^{-2} , and a 0.75 quantile of -14 W m^{-2} ; this contrasts the net heat flux which is approximately normally distributed. (See Supporting Information Figure S1 and

Text S3.) The decorrelation time scale is 3 to 4 days for each heat flux component reflecting the time scale of synoptic variability associated with episodic heat loss events. We emphasize the most extreme heat loss events in this region, specifically when daily mean turbulent heat loss exceeds 2σ below the mean (i.e. $<-144 \text{ W m}^{-2}$, see Figure 3). There are 29 days that meet this criterion all located in the negative tail of the turbulent heat flux probability density function in Supporting Information Figure S1; 7 of these days have daily mean turbulent heat loss exceeding 3σ below the mean, $<-193 \text{ W m}^{-2}$ (see Supporting Information Table S2). Of these 7 3σ heat loss events, 5 occurred in 2015 despite the large gap in winter data, while only 2 events occurred in 2016. These events were typically associated with strong relative wind speeds (northeastward) and large air-sea temperature and humidity differences (Figure 3b,c,d,e). We note that each 2σ turbulent heat loss event resulted in a negative net heat flux (and included the most extreme net heat fluxes); however, in seasons other than winter, Q_{SW} offsets the turbulent heat loss leading to weaker net heat loss.

The most striking feature of MLD variability is a large difference in wintertime MLD between the three years analyzed. In each year, MLD estimates from both Argo float and mooring data show a gradual mixed layer deepening from summer through early winter; however, 2015 and 2017 have much deeper winter mixed layers than 2016 (Figure 3f). The large range of Argo float winter MLDs (100 m to 500 m) in years with deep MLDs (2015 and 2017) shows spatial heterogeneity. Even so, the overall MLDs were substantially shallower in winter 2016 compared to winter 2015 in the broader Southeast Pacific (Supporting Information Figure S2). In late July through early October 2015, flanking mooring A and float MLD estimates reach 500 m. The 2σ and 3σ turbulent heat loss events in late winter 2015 suggest that frequent strong winter turbulent heat loss events are necessary for these deep MLDs. In contrast, in winter 2016, the profiler mooring and flanking mooring A observations show shallow MLDs (<300 m deep) consistent with the weak heat loss in this winter. Similar to winter 2015, winter 2017 float data show very deep mixed layers (up to 500 m).

Flanking mooring A CTDs show that the 2015 winter mixed layers exhibit the density of Southeast Pacific SAMW ($26.99\text{-}27.02 \text{ g cm}^{-3}$) described by *Holte et al.* [2012] and *Carter et al.* [2014] from mid-August through early October with MLDs exceeding 500 m (Figure 3g). The potential temperature was between 5.25 and 5.5°C , near the upper limit for Southeast Pacific SAMW [*Carter et al.*, 2014] (Supporting Information Figure S3). In 2016, SAMW formation was likely nonexistent in the density range $26.99\text{-}27.02 \text{ g cm}^{-3}$ due to lack of deep MLDs, low potential density ($26.8\text{-}26.85 \text{ g cm}^{-3}$), and high potential temperature ($6.0\text{-}6.5^\circ\text{C}$). Both winters had mixed layers within the SAMW practical salinity range as in *Holte et al.* [2012] ($34.08\text{-}34.20$ psu) with 2015 much saltier ($34.18\text{-}34.20$ psu) than 2016 ($34.08\text{-}34.12$ psu) (Supporting Information Figure S4).

We further analyze the drivers of extreme turbulent heat loss events in Figure 4. Daily turbulent heat flux as a function of wind direction and air temperature shows that heat loss events cluster around northeastward winds. Thus, advection of cold, dry Antarctic air, leading to large air-sea temperature and humidity (not shown) differences, is the prime driver of sensible and latent heat losses at the OOI site. There is a strong correlation of both air temperature and humidity with turbulent heat flux, with correlation coefficients of $r = 0.67$ and 0.79 , respectively ($p < 0.05$). In contrast, the correlation between SST and turbulent heat flux is weak ($r = 0.15$); thus, SST does not play a strong role in determining the heat exchange. Separation of observations by year (Figure 4b) and (Figure 4c) shows the absence of very cold air temperatures (below 2°C) in winter 2016, leading to few 2σ or 3σ heat loss events in this winter even in cases with strong northeastward winds.

To illustrate a typical synoptic regime that leads to episodic turbulent heat loss, we show the ERA-Interim daily averaged turbulent heat flux and atmospheric conditions in the Southeast Pacific on 6 August 2015 (Figure 4d,e,f). On this day, the daily averaged

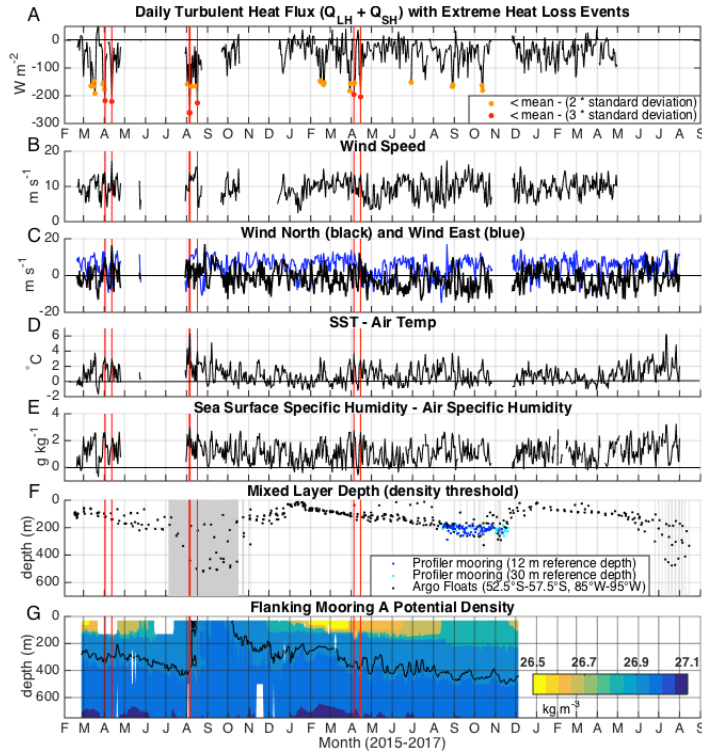


Figure 3. a) Daily turbulent heat flux ($Q_{LH} + Q_{SH}$) with 2σ and 3σ heat loss events (fluxes more than two standard deviations below the mean) labeled with orange points, while the red points and lines indicate heat loss events with fluxes more than three standard deviations below the mean; b) relative wind speed; c) northward (black) and eastward (blue) wind components; d) SST minus air temperature, e) sea surface specific humidity minus air specific humidity and f) MLDs from Argo floats (black) and the profiler mooring (blue for reference depths of 12 m from the surface mooring and cyan for reference depths of 30 m from flanking mooring A). Grey shading indicates when flanking mooring A and Argo float MLDs were >250 m. g) Daily average potential density from flanking mooring A with a black contour at 26.99 kg m^{-3} , the lower limit for SAMW from *Carter et al.* [2014].

turbulent heat loss observed at the surface mooring was -262 W m^{-2} , compared to -302 W m^{-2} from ERA-Interim (Figure 4d). The atmospheric regime during this heat loss event is typical of the majority of strong heat loss events. Strong, northeastward winds causing a large meridional deviation in isotherms of air temperature bring anomalously cold, dry air over the mooring location (Figure 4e). The northward winds are associated with cyclonic atmospheric circulation surrounding a low pressure system located southeast of the mooring (Figure 4f).

4 Discussion and Conclusions

The OOI surface mooring observations from February 2015 to August 2017 provide the first high-quality, year-round time series of air-sea heat fluxes from a SAMW formation region in the southeast Pacific sector of the Southern Ocean. Intense turbulent heat loss events are related to advection of cold, dry air masses mainly from the south, consistent with previous results from limited observations in the Southeast Pacific [*Holte et al.*, 2012]. These results have important implications for variability in anthropogenic CO₂ up-

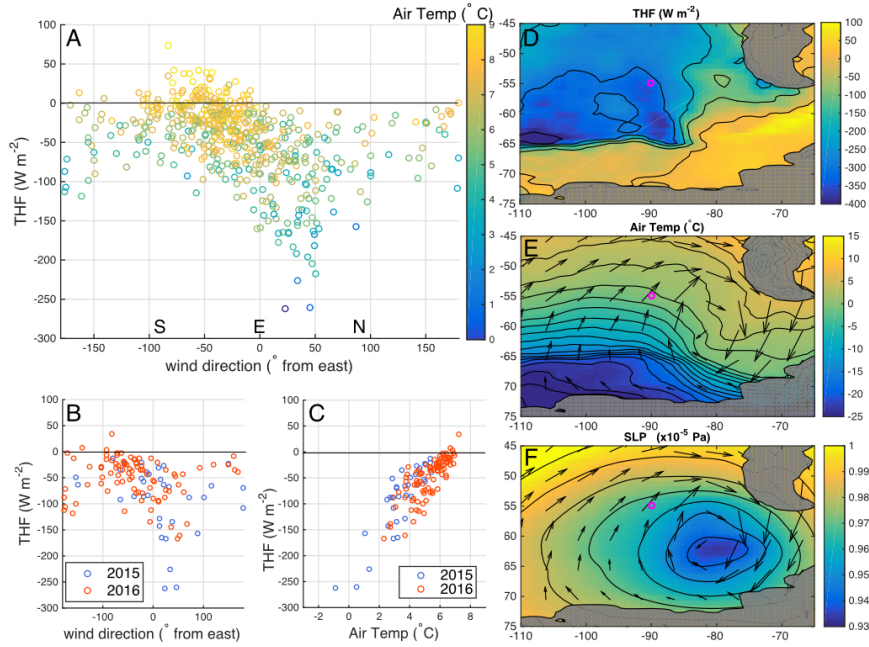


Figure 4. Turbulent heat loss event regimes. Scatter plot of: a) entire time series daily mean turbulent heat loss versus wind direction, colored by air temperature, b) winter (July, August, September) daily mean turbulent heat loss versus wind direction colored by year, c) winter daily mean turbulent heat loss versus air temperature colored by year; ERA-Interim: d) daily mean turbulent heat flux on August 6th, 2015, e) air temperature on same date (colors and black contours), and f) sea level pressure on same date (SLP, colors and contours). In e) and f) arrows show wind velocity vectors. In (d-f) magenta circles indicate the location of the mooring array.

take and storage in the oceans, as deep winter mixed layers and SAMW formation play a key role in these processes [Frölicher *et al.*, 2015].

The mooring observations show substantially stronger turbulent heat loss in late winter 2015 compared to 2016 (Figure 2); this is consistent with NCEP/NCAR (for which the monthly mean turbulent heat loss is -132 W m^{-2} in Aug 2015 and -58 W m^{-2} in Aug 2016). This difference in intensity of heat loss and corresponding mixed layer deepening in 2016 compared to 2015 was influenced by different climate conditions in these two years, including the Southern Annular Mode (SAM) and the El Niño Southern Oscillation (ENSO) indices (which Vivier *et al.* [2010] shows each exert a similar influence) (Supporting Information Figure S5) [Marshall and NCAR Staff, 2016]. In 2015, strong positive SAM persisted until austral spring; under such conditions, zonal winds drive strong Ekman transport of relatively cold water across the ACC, likely priming the region surrounding the mooring array for the formation of deep winter mixed layers [Tréguier *et al.*, 2010; Vivier *et al.*, 2010]. Naveira Garabato *et al.* [2009] showed that ENSO is a major driver of SST variability in this region, and thus the strong positive ENSO that peaked at the end of 2015 contributed to anomalously warm SSTs and air temperatures observed in winter 2016 that helped inhibit deep mixed layer formation.

Our observations can be compared with those from the SOFS mooring at 47°S , 142°E , south of Australia [Schulz *et al.*, 2012]. Both moorings lie north of the SAF in SAMW formation regions and experience heat loss on synoptic time scales from storms with northward wind components bringing relatively cold, dry air. Each exhibits asymmetric seasonal cycles with prolonged cooling periods and shorter heating periods. This

similarity suggests that these results may be applicable over a broader region on the northern edge of the ACC. However, the SOFS mooring has measured substantially stronger heat loss events than the OOI mooring (-470 W m^{-2} daily mean reported by Schulz *et al.* [2012]) and is also located in a region with deeper maximum climatological MLDs ($>700 \text{ m}$) [Holte *et al.*, 2017]. The higher SSTs due to the lower latitude and proximity to the warm, poleward Eastern Australian Current make the SOFS mooring region more susceptible to large air-sea temperature differences. A detailed comparison of concurrent data from the two moorings would be valuable but is beyond the scope of this work. Additionally, the impact of northward excursions of the SAF (and associated large SST gradients) at the OOI mooring location on heat flux variability is the subject of ongoing work.

The OOI Southern Ocean surface mooring data were not initially released on the Global Telecommunication System (GTS), and thus until 9 August 2017 were not assimilated into numerical weather prediction or reanalysis products. This means that an unbiased comparison between the mooring and reanalysis products is warranted to evaluate biases in these products. In cases where reanalysis fluxes compare reasonably well with the mooring data, longer reanalysis time series could provide further insight into the role of ENSO and SAM in interannual variability of wintertime heat loss in this region. Inclusion of the surface mooring data in the GTS after 9 August 2017 has significantly improved short-range forecasts produced by the European Centre for Medium-Range Weather Forecasts (ECMWF) (Peter Bauer, personal communication). This is particularly valuable as the mooring is proximate to Drake Passage, which is an area of critical ship operations. In addition, this mooring data (and hopefully a future mooring) is relevant for the Year of Polar Predictability, which will be intensely observing the Southern Hemisphere in early 2018 in order to improve polar weather predictions.

Thus, there are both scientific questions and immediate practical reasons for continuing mooring observations in this region. So far, the mooring observations have furthered our understanding of turbulent heat loss events and their relationship to mixed layer depths while aiding critical weather predictions. Ongoing observations will extend the time series into 2018 and subsequent studies are planned using these data to evaluate the accuracy of reanalysis products, develop our understanding of interannual variability, and establish the effects of climate change on this region.

Acknowledgments

S.E.O., L.D.T., S.T.G., and V.T. (at sea) were supported by the Southern Ocean Carbon and Climate Observations and Modeling Project under NSF PLR-1425989; V.T. and I.C. received significant support from NSF OCE-1357072. S.T.G. and I.C. were also supported by NSF OCE-1658001. S.A.J. is supported by the UK Natural Environment Research Council, including the ORCHESTRA grant (number NE/N018095/1). Flux data can be obtained from the NSF Ocean Observatories Initiative Data Portal, <http://ooinet.oceanobservatories.org>. Argo data were accessed using the USGODAE Argo GDAC Data Browser: http://www.usgodae.org/cgi-bin/argo_select.pl. The authors thank the OOI data management team for their support in working with the mooring data and thank Sebastian Bigorre and Marie Le Naour for helpful discussion.

References

- Bigorre, S. P., R. A. Weller, J. B. Edson, and J. D. Ware (2013), A surface mooring for air-sea interaction research in the Gulf Stream. Part II: Analysis of the observations and their accuracies, *Journal of Atmospheric and Oceanic Technology*, 30(3), 450–469.
- Bigorre, S., V. Tamsitt, M. Horn, J. Kemp, T. Thomas, L. Houghton, M. Ochs, and R. Sanger (2017). Southern Ocean 2 Deployment Cruise Report Ver 1-01, *Ocean Observatories Initiative*, Control Number: 3201-00203, Retrieved from <https://alfresco.oceanobservatories.org/alfresco/faces/jsp/browse/browse.jsp>.

- Bourassa, M. A., S. T. Gille, C. Bitz, D. Carlson, I. Cerovečki, C. A. Clayson, M. F. Cronin, W. M. Drennan, C. W. Fairall, R. N. Hoffman, et al. (2013), High-latitude ocean and sea ice surface fluxes: Challenges for climate research, *Bulletin of the American Meteorological Society*, 94(3), 403–423.
- Carter, B., L. Talley, and A. Dickson (2014), Mixing and remineralization in waters detrained from the surface into subantarctic mode water and antarctic intermediate water in the southeastern Pacific, *Journal of Geophysical Research: Oceans*, 119(6), 4001–4028.
- Cerovečki, I., and M. R. Mazloff (2016), The spatiotemporal structure of diabatic processes governing the evolution of SubAntarctic mode water in the Southern Ocean, *Journal of Physical Oceanography*, 46(2), 683–710.
- Cerovečki, I., L. D. Talley, M. R. Mazloff, and G. Maze (2013), Subantarctic mode water formation, destruction, and export in the eddy-permitting southern ocean state estimate, *Journal of Physical Oceanography*, 43(7), 1485–1511.
- Colbo, K., and R. A. Weller (2009), Accuracy of the imet sensor package in the subtropics, *Journal of Atmospheric and Oceanic Technology*, 26(9), 1867–1890.
- Curry, R., A. Alai, C. Basque, S. Caldwell, B. Guerro, C. Haskins, L. Houghton, J. Kuo, J. Mitchell, W. Ostrom, T. Thomas, G. Yonkoske (2017). Southern Ocean 3 Deployment Cruise Report Ver 1-00, *Ocean Observatories Initiative*, Control Number: 3201-00203, Retrieved from <https://alfresco.oceanobservatories.org/alfresco/faces/jsp/browse/browse.jsp>.
- da Silva, A. M., C. C. Young, and S. Levitus (1994), Atlas of surface marine data 1994, vol. 4: Anomalies of fresh water fluxes, *NOAA Atlas, NESDIS*, 9.
- de Boyer Montégut, C., G. Madec, A. S. Fischer, A. Lazar, and D. Iudicone (2004), Mixed layer depth over the global ocean: An examination of profile data and a profile-based climatology, *Journal of Geophysical Research*, 109, c12003, doi:10.1029/2004JC002378.
- Dee, D. P., S. M. Uppala, A. J. Simmons, P. Berrisford, P. Poli, S. Kobayashi, U. Andrae, M. A. Balmaseda, G. Balsamo, P. Bauer, et al. (2011), The ERA-Interim reanalysis: Configuration and performance of the data assimilation system, *Quarterly Journal of the Royal Meteorological Society*, 137(656), 553–597.
- Dufour, C. O., I. Frenger, T. L. Frölicher, A. R. Gray, S. M. Griffies, A. K. Morrison, J. L. Sarmiento, and S. A. Schlunegger (2015), Anthropogenic carbon and heat uptake by the ocean: Will the Southern Ocean remain a major sink?, *US Clivar Variations*, 13(4), 1–7.
- Edson, J. B., V. Jampana, R. A. Weller, S. P. Bigorre, A. J. Plueddemann, C. W. Fairall, S. D. Miller, L. Mahrt, D. Vickers, and H. Hersbach (2013), On the exchange of momentum over the open ocean, *Journal of Physical Oceanography*, 43(8), 1589–1610.
- Freeman, E., S. D. Woodruff, S. J. Worley, S. J. Lubker, E. C. Kent, W. E. Angel, D. I. Berry, P. Brohan, R. Eastman, L. Gates, et al. (2017), ICOADS Release 3.0: a major update to the historical marine climate record, *International Journal of Climatology*, 37(5), 2211–2232.
- Frölicher, T. L., J. L. Sarmiento, D. J. Paynter, J. P. Dunne, J. P. Krasting, and M. Winton (2015), Dominance of the Southern Ocean in anthropogenic carbon and heat uptake in CMIP5 models, *Journal of Climate*, 28(2), 862–886.
- Gille, S., S. Josey, and S. Swart (2016), New approaches for air-sea fluxes in the Southern Ocean, *Eos*, 97, doi:10.1029/2016EO052243.
- Hanawa, K., and L. D. Talley (2001), *In Ocean Circulation and Climate*, chap. Mode Waters, pp. 373–386, International Geophysics Series, Academic Press.
- Hartin, C. A., R. A. Fine, B. M. Sloyan, L. D. Talley, T. K. Chereskin, and J. Happell (2011), Formation rates of Subantarctic mode water and Antarctic intermediate water within the South Pacific, *Deep Sea Research Part I: Oceanographic Research Papers*, 58(5), 524–534.
- Holte, J., L. D. Talley, J. Gilson, and D. Roemmich (2017), An Argo mixed layer climatology and database, *Geophysical Research Letters*, 44, 5618–5626,

- doi:10.1002/2017GL073426.
- Holte, J. W., L. D. Talley, T. K. Chereskin, and B. M. Sloyan (2012), The role of air-sea fluxes in Subantarctic Mode Water formation, *Journal of Geophysical Research: Oceans*, *117*, C03040, doi:10.1029/2011JC007798.
- Hosom, D. S., R. A. Weller, R. E. Payne, and K. E. Prada (1995), The imet (improved meteorology) ship and buoy systems, *Journal of Atmospheric and Oceanic Technology*, *12*(3), 527–540.
- Ito, T., M. Woloszyn, and M. Mazloff (2010), Anthropogenic carbon dioxide transport in the Southern Ocean driven by Ekman flow, *Nature*, *463*(7277), 80–83.
- Iudicone, D., S. Speich, G. Madec, and B. Blanke (2008), The global conveyor belt from a southern ocean perspective, *Journal of Physical Oceanography*, *38*(7), 1401–1425.
- Josey, S. A., S. Gulev, and L. Yu (2013), *In Ocean Circulation and Climate 2nd Ed. A 21st century perspective*, vol. 103, chap. Exchanges through the ocean surface, pp. 115–140, Academic Press, doi:10.1016/B978-0-12-391851-2.00005-2.
- Kalnay, E., M. Kanamitsu, R. Kistler, W. Collins, D. Deaven, L. Gandin, M. Iredell, S. Saha, G. White, J. Woollen, et al. (1996), The NCEP/NCAR 40-year reanalysis project, *Bulletin of the American meteorological Society*, *77*(3), 437–471.
- Lenton, A., and R. J. Matear (2007), Role of the southern annular mode (SAM) in Southern Ocean CO₂ uptake, *Global Biogeochemical Cycles*, *21*(2), GB2016, doi:10.1029/2006GB002714.
- Marshall, G. and National Center for Atmospheric Research Staff (Eds). Last modified 10 Jun 2016. "The Climate Data Guide: Marshall Southern Annular Mode (SAM) Index (Station-based)." Retrieved from <https://climatedataguide.ucar.edu/climate-data/marshall-southern-annular-mode-sam-index-station-based>.
- McCartney, M. (1977), Subantarctic mode water, *A Voyage of Discovery: George Deacon 70th Anniversary Volume, Supplement to Deep Sea Research*, M. Angel, 103–119.
- McCartney, M. S. (1982), The subtropical recirculation of mode waters, *J. Mar. Res.*, *40*(436), 427–464.
- Mikaloff Fletcher, S. E., N. Gruber, A. R. Jacobson, S. C. Doney, S. Dutkiewicz, M. Gerber, M. Follows, F. Joos, K. Lindsay, D. Menemenlis, et al. (2006), Inverse estimates of anthropogenic CO₂ uptake, transport, and storage by the ocean, *Global Biogeochemical Cycles*, *20*(2), GB2002, doi:10.1029/2005GB002530.
- Naveira Garabato, A. C., L. Jullion, D. P. Stevens, K. J. Heywood, and B. A. King (2009), Variability of Subantarctic Mode Water and Antarctic Intermediate Water in the Drake Passage during the late-twentieth and early-twenty-first centuries, *Journal of Climate*, *22*(13), 3661–3688.
- Roemmich, D., G. C. Johnson, S. Riser, R. Davis, J. Gilson, W. B. Owens, S. L. Garzoli, C. Schmid, and M. Ignaszewski (2009), The Argo Program: Observing the global oceans with profiling floats, *Oceanography*, *22*, 24–33.
- Sabine, C. L., R. A. Feely, N. Gruber, R. M. Key, K. Lee, J. L. Bullister, R. Wanninkhof, C. S. Wong, D. W. R. Wallace, B. Tilbrook, et al. (2004), The oceanic sink for anthropogenic CO₂, *Science*, *305*(5682), 367–371.
- Schulz, E. W., S. A. Josey, and R. Verein (2012), First air-sea flux mooring measurements in the Southern Ocean, *Geophysical Research Letters*, *39*(16), L16606, doi:10.1029/2012GL052290.
- Simmons, A., S. Uppala, D. Dee, and S. Kobayashi (2007), Era-interim: New ecmwf reanalysis products from 1989 onwards, *110-Winter 2006/07*, 11 pp.
- Sokolov, S., and S. R. Rintoul (2009), Circumpolar structure and distribution of the antarctic circumpolar current fronts: 1. mean circumpolar paths, *Journal of Geophysical Research: Oceans*, *114*(C11).
- Talley, L. D., G. L. Pickard, W. J. Emery, and J. H. Swift (2011), *Descriptive Physical Oceanography: An Introduction (6th Edition)*, Elsevier, Boston, 560pp.
- Tréguier, A.-M., J. Le Sommer, J.-M. Molines, and B. De Cuevas (2010), Response of the southern ocean to the southern annular mode: Interannual variability and multidecadal

- trend, *Journal of Physical Oceanography*, 40(7), 1659–1668.
- Vivier, F., D. Iudicone, F. Busdraghi, and Y.-H. Park (2010), Dynamics of sea-surface temperature anomalies in the southern ocean diagnosed from a 2d mixed-layer model, *Climate Dynamics*, 34(2-3), 153–184.
- Weller, R. A., S. P. Bigorre, J. Lord, J. D. Ware, and J. B. Edson (2012), A surface mooring for air–sea interaction research in the Gulf Stream. Part I: Mooring design and instrumentation, *Journal of Atmospheric and Oceanic Technology*, 29(9), 1363–1376.
- Weller, B., D. Gassier, K. Newhall, B. Pietro, D. Wellwood, E. Morris, J. Ryder, G. Chavez, A. Alai, and J. Lund (2015). Southern Ocean 1 Deployment Cruise Report Ver 1-00, *Ocean Observatories Initiative*, Control Number: 3201-00103, Retrieved from <https://alfresco.oceanobservatories.org/alfresco/faces/jsp/browse/browse.jsp>.